Electrically Switchable and Tunable Rashba-Type Spin Splitting in Covalent Perovskite Oxides

Julien Varignon,[1,*] Jacobo Santamaria,[2,1] and Manuel Bibes[1]
[1]Unité Mixte de Physique, CNRS, Thales, Université Paris Sud, Université Paris-Saclay, 91767, Palaiseau, France
[2]Laboratorio de Heteroestructuras con aplicacion en Spintronica, Unidad Asociada CSIC/Universidad Complutense de Madrid, Sor Juana Inés de la Cruz, 3, 28049 Madrid, Spain, Instituto de Magnetismo Aplicado, Universidad Complutense de Madrid, 28040 Madrid Spain

(Received 18 June 2018; published 22 March 2019)

In transition-metal perovskites (ABO_3) most physical properties are tunable by structural parameters such as the rotation of the BO_6 octahedra. Examples include the Néel temperature of orthoferrites, the conductivity of mixed-valence manganites, or the band gap of rare-earth scandates. Since oxides often hold large internal electric dipoles and can accommodate heavy elements, they also emerge as prime candidates to display Rashba spin-orbit coupling, through which charge and spin currents may be efficiently interconverted. However, despite a few experimental reports in $SrTiO_3$-based interface systems, the Rashba interaction has been little studied in these materials, and its interplay with structural distortions remains unknown. In this Letter, we identify a bismuth-based perovskite with a large, electrically switchable Rashba interaction whose amplitude can be controlled by both the ferroelectric polarization and the breathing mode of oxygen octahedra. This particular structural parameter arises from the strongly covalent nature of the Bi-O bonds, reminiscent of the situation in perovskite nickelates. Our results not only provide novel strategies to craft agile spin-charge converters but also highlight the relevance of covalence as a powerful handle to design emerging properties in complex oxides.

DOI: 10.1103/PhysRevLett.122.116401

Spintronics exploits the spin degree of freedom of carriers in addition to their charge, giving rise to a very broad range of electronic applications including magnetic memories or magnetic sensors [1,2]. Traditionally, it has relied on the exchange interaction of electrons with local magnetic moments of a ferromagnet to generate spin currents. Usually, the ferromagnets are simple transition-metal elements such as Co, Ni, or their alloys whose magnetization is used to store nonvolatile information. Nevertheless, the control of their magnetization typically requires large energies and generates undesired magnetic fields hindering a high densification of devices. In the search for lower power spintronic devices, the spin-orbit interaction (SOI) has been identified as a promising pathway to generate spin currents from charge currents and vice versa. The two phenomena at the core of this branch of spintronics, also called spin-orbitronics, are the spin Hall effect (SHE) [3,4] and inverse spin Hall effect (ISHE) [5,6]. For instance, the former effect allows efficient charge-to-spin current conversion in nonmagnetic materials based on heavy elements [7], therefore alleviating the need for ferromagnets to generate spin currents.

More recently, renewed interest for SOI based applications arose thanks to the Rashba effect [8]. In materials lacking inversion symmetry, the interplay between the electric field and the SOI lifts the degeneracy of electronic bands according to their spin. For a material exhibiting a polar axis oriented along the z direction, Rashba proposed the following spin-orbit interaction:

$$H_R = \alpha_R(\sigma_x k_y - \sigma_y k_x), \tag{1}$$

where α_R is the Rashba coefficient—proportional to the spin-orbit strength of the material λ_{SO} and to the magnitude of the electric field, σ_i ($i = x, y$) are Pauli matrices and k_j ($j = x, y$) is the momentum of the electron. The Rashba interaction leads to a spin locking of electrons according to their momentum $\vec{k}$ enabling efficient spin-to-charge current interconversions through Edelstein and inverse Edelstein effects [9,10]. Although originally formulated at interfaces and surfaces [11–14], the Rashba interaction is now generalized to noncentrosymmetric bulk materials [15–18], although it may coexist with the Dresselhaus interaction [19].

In the context of SOI related devices, ABO_3 oxide perovskites remain largely unexplored although they are promising candidates for applications [14,17,18,20–24]. They encompass a wealth of properties—including ferroelectricity and magnetism—and functionalities originating from the coupling of their structural, electronic, and magnetic degrees of freedom [25]. Most notably, the lattice distortions usually control the properties of the perovskite, such as the metal-insulator phase transition temperature in rare-earth nickelates [26,27], the Néel temperature of

orthoferrites [28,29], or the band gap value of rare-earth scandates [30,31]. Being largely ionic in most cases, many oxide perovskites host large internal electric dipoles. Moreover, they can also accommodate heavy elements, an important aspect for SOI based applications. So far, $BiAlO_3$ has been proposed theoretically to be the first oxide exhibiting ferroelectricity and Rashba physics [17]—although this coexistence was already observed in the semiconductor GeTe [16]. While $BiAlO_3$ comprises a heavy element and a large ferroelectric polarization—estimated around 90 $\mu C\,cm^{-2}$—, the computed Rashba coefficient α_R remains relatively moderate—around 0.39 and 0.74 eV Å—although comparable to conventional systems such as (111) oriented Bi [32]. In fact, other ingredients such as a narrow band gap and/or similar atomic and orbital characters for the electronic states located around the Fermi level are proposed to be additional key ingredients for reaching large α_R [33]. Covalent oxides that are characterized by a strong hybridization of B cations and O anions electronic states around the Fermi level, are therefore an ideal platform to engineer materials undergoing large Rashba effects. Furthermore, oxides are usually characterized by numerous lattice distortions but the role of the latter on the Rashba physics remains unexplored.

In this Letter, we use *first-principles* simulations to identify the existence of large Rashba effects in a ferroelectric phase reachable by epitaxial strain in the covalent oxide strontium bismuthate $SrBiO_3$. We show that the chiral spin texture of the Fermi contours reverses upon switching polarization. Furthermore, we reveal that the amplitude of the Rashba coefficient is tunable by a lattice distortion strongly connected to band dispersion and to the level of hybridization between B and O electronic states. Our results therefore highlight a new pathway to control and optimize the Rashba interaction in oxides, further revealing the potential of these materials for spin-orbitronics [20,21].

Strontium bismuthate $Sr^{2+}Bi^{4+}O_3$ is an insulator adopting a monoclinic $P2_1/n$ symmetry at low temperature [34,35]. The ground state structure is characterized by the usual oxygen cage rotations appearing in perovskites, $a^-a^-c^+$ antiferrodistortive motions in Glazer's notation, as well as by a breathing of the oxygen cage octahedra distortion B_{oc} [34,35]. The latter distortion produces a rocksaltlike pattern of large and small O_6 groups resulting in Bi sites splitting. In the following, Bi cations sitting in compressed or short bonds (extended or long bonds) O_6 groups are labeled Bi_S (Bi_L). Since $SrBiO_3$ shares several features with rare-earth nickelates $RNiO_3$, the appearance of B_{oc} in bismuthates is sometimes interpreted in terms of ionic charge disproportionation of the unstable Bi^{4+} valence state to the more stable $Bi_L^{3+} + Bi_S^{3+}$ electronic configurations in the insulating phase [36–38]. Alternatively, it is also proposed to be a consequence of charge transfer effects from O anions to Bi cations [39]. Nevertheless, Tonnhauser and Rabe demonstrated that the appearance of B_{oc} is responsible for the band gap opening in bismuthates [40].

Although very similar to rare-earth nickelates, bismuthates also exhibit many other striking properties such as high T_c superconductivity upon hole doping [35,41–44] or possible topological surface states accessible upon electron doping [45]. The latter point highlights the strength of the SOI in these materials, being *de facto* an ideal playground to study theoretically the interplay between lattice distortions, covalence, and spin-orbit related phenomena.

First-principles calculations were carried out with density functional theory (DFT) using the Vienna *ab initio* simulation package (VASP) [46,47]. We used the PBE functional revised for solids [48] with a cutoff energy of 500 eV and a $6 \times 6 \times 4$ ($4 \times 4 \times 4$) Monkhorst-Pack k-point mesh for 20 (40) atom unit cells. We used projector augmented waves (PAW) potentials [49] for core electrons with the following valence electron configurations: $4s^2 4p^6 5s^2$ (Sr), $6s^2 6p^3$ (Bi), and $2s^2 2p^4$ (O). Geometry optimizations were performed until forces are lower than 0.01 meV $Å^{-1}$ without spin-orbit interaction included unless stated. Born effective charges and phonon frequencies were computed with the density functional perturbation theory [50,51]. Band structures and spin textures were plotted with the PyProcar script [52]. Maximally localized Wannier functions (MLWFs) were extracted with the Wannier90 package [53–55].

We first inspect the properties of bulk strontium bismuthate. Geometry relaxation yields an insulating monoclinic $P2_1/n$ ground state with a band gap of 0.3 eV, other polymorphs observed experimentally at higher temperature —$Fm\bar{3}m$, $R\bar{3}c$, or I_2/m symmetries—are found higher in energy. Our optimized lattice parameters ($a = 5.9400$ Å, $b = 6.1365$ Å, $c = 8.4859$ Å, and $\beta = 90.0597°$) are found in very good agreement with experiments ($a_{exp} = 5.9480$ Å, $b_{exp} = 6.0951$ Å, $c_{exp} = 8.4854$ Å, and $\beta_{exp} = 90.063°$) from Ref. [35], yielding 0.55% of error on the total volume. Regarding the electronic structure of the material, we identify a strongly hybridized electronic structure between Bi s and O p levels with an absence of charge ordering of the Bi cations. Just as in previous theoretical studies [39,56], this is due to a charge transfer of O p levels to Bi s states, yielding Bi_L $6s^2$ and Bi_S $6s^2\underline{L}^2$ electronic structures where the notation $\underline{L}^2$ labels two ligand holes (see Supplemental Material [57] for further details).

Having now established that the structural and electronic properties of $SrBiO_3$ are in good agreement with experiments and recent theoretical works, we now turn our attention to spin-orbit related phenomena. When including the spin-orbit interaction in the calculation, we do not observe any sizable effect on the ground state properties, suggesting a marginal SOI in this material. However, the fact that $SrBiO_3$ is paraelectric in its bulk hinders possible

Rashba phenomena. We, however, observe the existence of a ferroelectric phonon mode at relatively low frequency ($\omega_{FE} \simeq 50\ cm^{-1}$) in the bulk. Therefore, through the coupling of this phonon mode with epitaxial strain [58], one may expect to unlock ferroelectricity in $SrBiO_3$. This is reinforced by the ability of Bi-based oxide perovskites to exhibit ferroelectricity in bulk or under epitaxial strain. Since the pseudocubic lattice parameter of $SrBiO_3$ is rather large ($a_{pc} \simeq 4.26$ Å), we only explored the effect of a compressive strain in our simulations. Additionally, the SOI having marginal effect on the structural aspect of the bismuthate, we ignored it during geometry relaxation under strain.

Figure 1 reports the energy of the most stable structures found in the calculations as a function of the substrate lattice parameter (lower scale) or compressive strain value (upper scale) [59]. Between 0% and 5% of compression, $SrBiO_3$ is a paraelectric insulator adopting a $P\bar{1}$ structure described by a $a^-a^-c^+$ oxygen cage rotation patterns and a breathing of O_6 groups (all ferroelectric phases tested are relaxing back to a centrosymmetric space group, e.g., $P1$ relaxes back to $P-1$). This structure is equivalent to the bulk except that the in-phase oxygen cage rotation axis is aligned along the substrate normal—such a growth orientation is sometimes referred to c-$P2_1/n$, the notation c-indicating that the c axis is aligned along the substrate normal [60]. Beyond 5% of compression, the ground state becomes ferroelectric and is associated with a $P1$ structure exhibiting the aforementioned structural distortions plus a spontaneous polarization in all three directions. Focusing on the structure obtained at 6.1% of compressive strain—i.e., $a_{substrate} = 4$ Å—, $SrBiO_3$ develops a polarization of 12.65 $\mu C\,cm^{-2}$ ($P_x = 9.64$, $P_y = 2.73$, $P_z = -7.73$ in a pseudo-$P2_1/n$ 20-atom unit cell setting, c being the long axis) approaching the value of the popular ferroelectric $BaTiO_3$.

When including the SOI in the ferroelectric phase, we now observe several splittings of the bands located above the Fermi level E_F [see Fig. 2(a)] in all reciprocal directions due to the presence of polarization along the three Cartesian axes. Energy splittings are observed at the bottom of the conduction band at the D point, although the largest energy splitting is observed at the Γ point 2 eV above E_F. Proper inspection of the spin flavor of bands along the k_z direction (i.e., centered around the D point at the bottom of the conduction band) reveal that their degeneracy is lifted

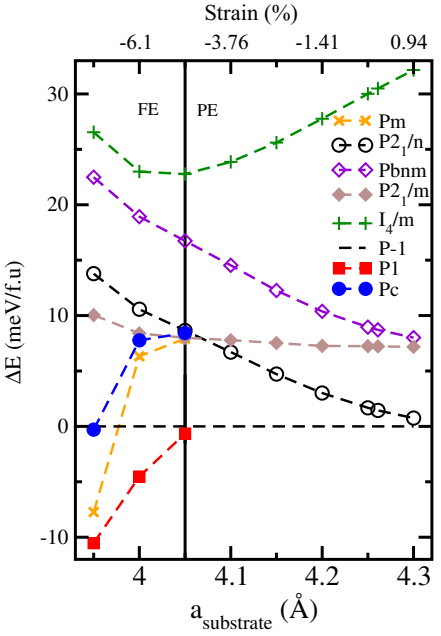

FIG. 1. Energy differences in meV per formula units (meV/f.u) between the different metastable phases as a function of the substrate lattice parameter (in Å, lower scale) or strain value (in %, upper scale). The reference energy is set to the $P-1$ structure energy (dashed horizontal black line). The vertical line represents the boundary between the ferroelectric (FE) and paraelectric (PE) phases.

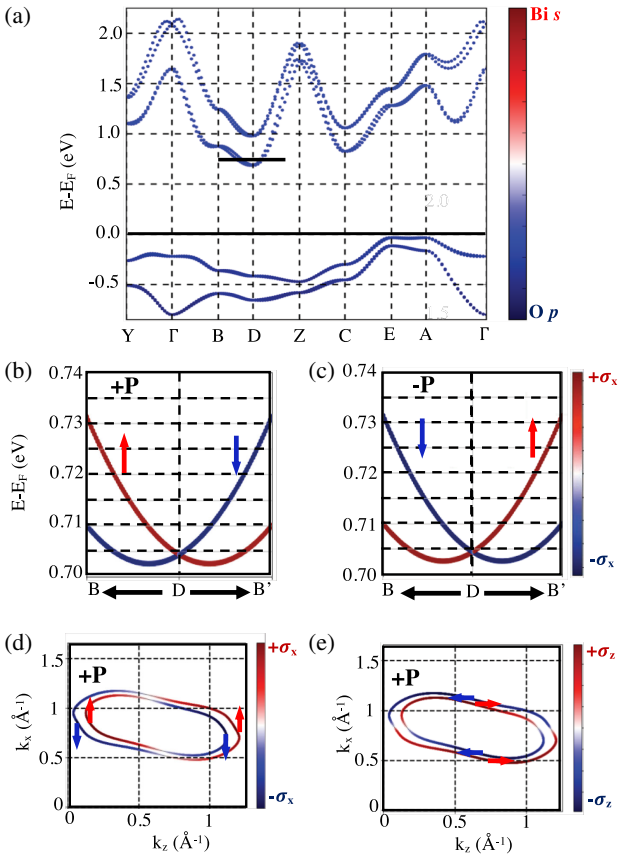

FIG. 2. Electronic properties of the ferroelectric ground state of $SrBiO_3$ at 6.1% of compressive strain. (a) Orbital projected [on O p (blue character) and Bi s (red character) states] band structure in a monoclinic $P2_1/n$ setting. The Fermi level is set to 0 eV. (b) and (c) Bands projected on the $\pm\sigma_x$ component along the $(+1/2, 0, 0)$ to $(+1/2, 0, 1)$ direction for $+P$ (b) or $-P$ (c) spontaneous polarization. (d) and (e) Spin textures in the (k_z, k_x) plan obtained at $E = +0.75$ eV when projecting on the $\pm\sigma_x$ (d) or $\pm\sigma_z$ (e) spin component for a positive spontaneous polarization.

according to the spin direction as illustrated by Figs. 2(b) and 2(c). Looking at spin textures in the (k_z, k_x) planes represented in Figs. 2(d)–2(e), we clearly observe two energy contours with clockwise (outer contour) and counterclockwise (inner contour) spin locking of electrons with respect to their momentum following Eq. (1) (a similar effect is observed for states located 2 eV above the Fermi level, see Supplemental Material [57]). Consequently, the ferroelectric phase of $SrBiO_3$ reached under compressive epitaxial strain undergoes a Rashba interaction. Approximating the Rashba coefficient by $\alpha_R = 2E_R/k_R$, where E_R is the energy splitting of the bands with respect to the high-symmetry position and k_R is the momentum offset, we estimate Rashba coefficients of 0.944 and 0.845 eV Å along the $D - Z$ and $D - B$ directions, respectively, at the bottom of the conduction bands (8.397 eV Å for states 2 eV above the Fermi level). The Rashba coefficients appearing at the conduction band minimum are thus comparable to values computed in $BiAlO_3$ [17] or observed in heavy metals such as (111)-oriented Bi [32].

We now turn our attention to the possible functionalization of the Rashba interaction in this ferroelectric material. First, as inferred by Figs. 2(b) and 2(c), switching the polarization reverses the spin textures, therefore allowing their nonvolatile electrical control. By freezing different amplitudes of the ferroelectric distortion while keeping other distortions to their ground state amplitude, we observe a linear dependence of α_R with the ferroelectric mode amplitude [see Fig. 3(a)], in agreement with its dependence with the electric field. The functionality was already proposed theoretically in GeTe [16] or in $BiAlO_3$ [17]. A key aspect of the bismuthate is the strong relationship between the breathing mode B_{oc} and electronic properties. Although B_{oc} is found to open the band gap in the ferroelectric phase upon its condensation in our simulations—all other lattice distortions are fixed to their ground state amplitude—, it also controls the amplitude of the Rashba coefficient as inferred by Figs. 3(b)–3(d). Consequently, at odds with usual assumptions, the Rashba coefficient is not only sensitive to the spin-orbit strength λ_{SO} and the electric field amplitude, but it can also be strongly related to structural distortions altering the band dispersions and the level of hybridization between the B site cation and O states [61]. For instance, at the conduction band minimum, reducing the breathing mode amplitude could increase the Rashba parameter to 1.68 eV Å instead of 0.845 eV Å for the ground state structure. The latter observation is in close agreement with the work of Bahramy *et al.* highlighting that hybridized electronic states around E_F were a key aspect for large α_R [33]. We emphasize that similar observations are drawn for states located 2 eV above the Fermi level (see Supplemental Material [57].)

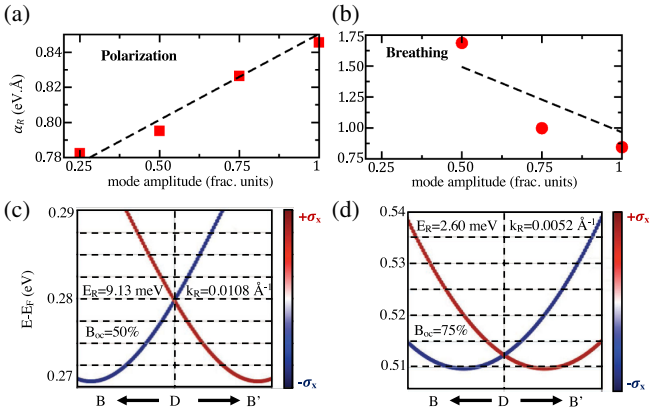

FIG. 3. Evolution of the Rashba coefficient when freezing different amplitudes of the polar distortion (a) and the breathing of the oxygen cage octahedra (b). (c) and (d) Bands projected on the $\pm\sigma_x$ component along the $(+1/2, 0, 0)$ to $(+1/2, 0, +1)$ direction for different amplitudes of the breathing distortion. We emphasize that all other lattice distortions are fixed to their amplitude appearing in the ferroelectric ground state.

In conclusion, we have predicted Rashba spin splittings in the covalent oxide perovskite $SrBiO_3$ with Rashba coefficients α_R that are strongly related to lattice distortions irrespective of the amplitude of the electric field or of the spin-orbit interaction. The Rashba physics being at the core of the most recent spin-orbitronics based applications, our work unveils new pathways to optimize and control α_R through the subtle interplay between lattice and electronic degrees of freedom appearing in oxide perovskites.

This work has been supported by the European Research Council (ERC) Consolidator Grant MINT under the Contract No. 615759. Calculations took advantage of the Occigen machines through the DARI project EPOC No. A0020910084 and of the DECI resource FIONN in Ireland at Irish Centre for High-End Computing (ICHEC) through the PRACE project FiPSCO. J. V. acknowledges technical help from Adam Ralph from ICHEC.

*julien.varignon@gmail.com

[1] C. Chappert, A. Fert, and F. N. VanDau, Nat. Mater. **6**, 813 (2007).
[2] S. Manipatruni, D. E. Nikonov, R. Ramesh, H. Li, and I. A. Young, arXiv:1512.05428v2.
[3] M. I. D'yakonov and V. I. Perel, JETP Lett. **13**, 467 (1971).
[4] Y. K. Kato, R. C. Myers, A. C. Gossard, and D. D. Awschalom, Science **306**, 1910 (2004).
[5] H. Zhao, E. J. Loren, H. M. van Driel, and A. L. Smirl, Phys. Rev. Lett. **96**, 246601 (2006).
[6] K. Ando and E. Saitoh, Nat. Commun. **3**, 629 (2012).
[7] L. Liu, C.-F. Pai, Y. Li, H. W. Tseng, D. C. Ralph, and R. A. Buhrman, Science **336**, 555 (2012).
[8] Y. A. Bychkov and E. I. Rashba, JETP Lett. **39**, 78 (1984).
[9] V. M. Edelstein, Solid State Commun. **73**, 233 (1990).
[10] J. C. Rojas Sánchez, L. Vila, G. Desfonds, S. Gambarelli, J. P. Attané, J. M. Teresa, C. Magén, and A. Fert, Nat. Commun. **4**, 2944 (2013).
[11] C. R. Ast, J. Henk, A. Ernst, L. Moreschini, M. C. Falub, D. Pacilé, P. Bruno, K. Kern, and M. Grioni, Phys. Rev. Lett. **98**, 186807 (2007).
[12] T. Aruga, J. Electron Spectrosc. Relat. Phenom. **201**, 74 2015.
[13] K. Yaji, Y. Ohtsubo, S. Hatta, H. Okuyama, K. Miyamoto, T. Okuda, A. Kimura, H. Namatame, M. Taniguchi, and T. Aruga, Nat. Commun. **1**, 17 (2010).
[14] E. Lesne, Y. Fu, S. Oyarzún, J.-C. Rojas-Sánchez, D. C. Vaz, H. Naganuma, G. Sicoli, J.-P. Attané, M. Jamet, E. Jacquet, J.-M. Georges, A. Barthélémy, H. Jaffres, A. Fert, M. Bibes, and L. Vila, Nat. Mater. **15**, 1261 (2016).
[15] K. Ishizaka *et al.*, Nat. Mater. **10**, 521 (2011).
[16] D. Di Sante, P. Barone, R. Bertacco, and S. Picozzi, Adv. Mater. **25**, 509 (2013).
[17] L. G. D. da Silveira, P. Barone, and S. Picozzi, Phys. Rev. B **93**, 245159 (2016).
[18] J. He, D. Di Sante, R. Li, X.-Q. Chen, J. M. Rondinelli, and C. Franchini, Nat. Commun. **9**, 492 (2018).
[19] G. Dresselhaus, Phys. Rev. **100**, 580 (1955).
[20] J. Varignon, L. Vila, A. Barthélémy, and M. Bibes, Nat. Phys. **14**, 322 (2018).
[21] D. C. Vaz, A. Barthélémy, and M. Bibes, Jpn. J. Appl. Phys. **57**, 0902A4 (2018).
[22] A. C. Garcia-Castro, M. G. Vergniory, E. Bousquet, and A. H. Romero, Phys. Rev. B **93**, 045405 (2016).
[23] K. Yamauchi, P. Barone, T. Shishidou, T. Oguchi, and S. Picozzi, Phys. Rev. Lett. **115**, 037602 (2015).
[24] K. Yamauchi, P. Barone, and S. Picozzi, Phys. Rev. B **95**, 035146 (2017).
[25] P. Zubko, S. Gariglio, M. Gabay, P. Ghosez, and J.-M. Triscone, Annu. Rev. Condens. Matter Phys. **2**, 141 (2011).
[26] M. L. Medarde, J. Phys. Condens. Matter **9**, 1679 (1997).
[27] A. Mercy, J. Bieder, J. Iñiguez, and P. Ghosez, Nat. Commun. **8**, 1677 (2017).
[28] W. C. Koehler and E. O. Wollan, J. Phys. Chem. Solids **2**, 100 (1957).
[29] W. C. Koehler, E. O. Wollan, and M. K. Wilkinson, Phys. Rev. **118**, 58 (1960).
[30] H. M. Christen, Appl. Phys. Lett. **88**, 262906 (2006).
[31] Seung-Gu Lim, Stas Kriventsov, and Thomas N. Jackson, J. Appl. Phys. **91**, 4500 (2002).
[32] Y. M. Koroteev, G. Bihlmayer, J. E. Gayone, E. V. Chulkov, S. Blügel, P. M. Echenique, and Ph. Hofmann, Phys. Rev. Lett. **93**, 046403 (2004).
[33] M. S. Bahramy, R. Arita, and N. Nagaosa, Phys. Rev. B **84**, 041202(R) (2011).
[34] B. J. Kennedy, C. J. Howard, K. S. Knight, Z. Zhang, and Q. Zhou, Acta Crystallogr. Sect. B **62**, 537 (2006).
[35] S. M. Kazakov, C. Chaillout, P. Bordet, J. J. Capponi, M. Nunez-Regueiro, A. Rysak, J. L. Tholence, P. G. Radaelli, S. N. Putilin, and E. V. Antipov, Nature (London) **390**, 148 (1997).
[36] D. E. Cox and A. W. Sleight, Solid State Commun. **19**, 969 (1976).
[37] R. P. S. M. Lobo and F. Gervais, Phys. Rev. B **52**, 13294 (1995).
[38] R. P. S. M. Lobo and F. Gervais, Solid State Commun. **98**, 61 (1996).
[39] K. Foyevtsova, A. Khazraie, I. Elfimov, and G. A. Sawatzky, Phys. Rev. B **91**, 121114 (2015).
[40] T. Thonhauser and K. M. Rabe, Phys. Rev. B **73**, 212106 (2006).
[41] H. Sato, S. Tajima, H. Takagi, and S. Uchida, Nature (London) **338**, 241 (1989).
[42] A. W. Sleight, J. L. Gillson, and P. E. Bierstedt, in *Ten Years of Superconductivity: 1980–1990* (Springer, New York, 1993), pp. 257–258.
[43] K. H. Kim, C. U. Jung, T. W. Noh, and S. C. Kim, Phys. Rev. B **55**, 15393 (1997).
[44] S. M. Kazakov, C. Chaillout, P. Bordet, J. J. Capponi, M. Nunez-Regueiro, A. Rysak, J. L. Tholence, P. G. Radaelli, S. N. Putilin, and E. V. Antipov, Nature (London) **390**, 148 (1997).
[45] B. Yan, M. Jansen, and C. Felser, Nat. Phys. **9**, 709 (2013).
[46] G. Kresse and J. Hafner, Phys. Rev. B **47**, 558 (1993).
[47] G. Kresse and J. Furthmüller, Comput. Mater. Sci. **6**, 15 (1996).
[48] J. P. Perdew, A. Ruzsinszky, Gá. I. Csonka, O. A. Vydrov, G. E. Scuseria, L. A. Constantin, X. Zhou, and K. Burke, Phys. Rev. Lett. **100**, 136406 (2008).
[49] P. E. Blöchl, Phys. Rev. B **50**, 17953 (1994).
[50] S. Baroni, S. de Gironcoli, A. Dal Corso, and P. Giannozzi, Rev. Mod. Phys. **73**, 515 (2001).
[51] X. Gonze and C. Lee, Phys. Rev. B **55**, 10355 (1997).
[52] A. H. Romero and F. Munoz, http://sourceforge.net/p/pyprocar/PyPROCAR/HEAD/tree/.
[53] A. Mostofi, J. R. Yates, Y.-S. Lee, I. Souza, D. Vanderbilt, and N. Marzari, Comput. Phys. Commun. **178**, 685 (2008).
[54] N. Marzari and D. Vanderbilt, Phys. Rev. B **56**, 12847 (1997).
[55] I. Souza, N. Marzari, and D. Vanderbilt, Phys. Rev. B **65**, 035109 (2001).
[56] G. M. Dalpian, Q. Liu, J. Varignon, M. Bibes, and A. Zunger, Phys. Rev. B **98**, 075135 (2018).
[57] See Supplemental Material at http://link.aps.org/supplemental/10.1103/PhysRevLett.122.116401 for further information, which includes Refs. [39,53–56].
[58] J. Varignon, N. C. Bristowe, E. Bousquet, and Ph. Ghosez, C.R. Phys. **16**, 153 (2015).
[59] We have tested several structures combining different oxygen cage rotation patterns and/or breathing distortion B_{oc}

and/or polar axes. Two growth orientations were used with either the a and b lattice parameters aligned at 45° of the a_{sub} and b_{sub} substrate lattice parameters or the c lattice parameter along the substrate. The eight most stable structures identified in the calculations are the following: $P2_1/n$ $(a^-a^-c^+ + B_{\mathrm{oc}})$, Pc $(a^-a^-c^+ + B_{\mathrm{oc}} + P_xP_yP_z)$, $Pbnm$ $(a^-a^-c^+)$, $P2_1/m$ $(a^+a^-c^-)$, Pm $(a^+a^-c^- + P_z)$, $P\bar{1}$ $(a^+a^-c^- + B_{\mathrm{oc}})$, and $P1$ $(a^+a^-c^- + B_{\mathrm{oc}} + P_xP_yP_z)$.

[60] The $P\bar{1}$ and $P1$ structures grow with the in-phase rotation axis along the substrate. We therefore have to use a 40-atom unit cell to model the constraint in our calculations. Nevertheless, results regarding band structures and polarizations are reported with respect to a 20-atom unit cell where the c axis is the long axis of the perovskite.

[61] Through the condensation of the breathing distortion in the ferroelectric ground state achieved under compressive strain, the asymmetry of the sphere integrated charges between Bi_S and Bi_L increases from $0e$ to $0.44e$, rather suggesting a strong modification of the electronic structure.

[62] D. G. Schlom, L.-Q. Chen, C. J. Fennie, V. Gopalan, D. A. Muller, X. Pan, R. Ramesh, and R. Uecker, MRS Bull. **39**, 118 (2014).

[63] D. Sando, A. Barthélémy, and M. Bibes, J. Phys. Condens. Matter **26**, 473201 (2014).

[64] G. Kim, M. Neumann, M. Kim, M. D. Le, T. D. Kang, and T. W. Noh, Phys. Rev. Lett. **115**, 226402 (2015).

[65] D. T. Harris, N. Campbell, R. Uecker, M. Bruützam, D. G. Schlom, A. Levchenko, M. S. Rzchowski, and C.-B. Eom, Phys. Rev. Mater. **2**, 041801(R) (2018).

[66] J. Junquera and P. Ghosez, Nature (London) **422**, 506 (2003).

[67] Z. Liao *et al.*, Nat. Mater. **15**, 425 (2016).